Superconducting ground state study of the valence-skipped compound $AgSnSe_2$

A. Kataria,[1] Arushi,[1] S. Sharma,[2] T. Agarwal,[1] M. Pula,[2] J. Beare,[2] S. Yoon,[3,4] Y. Cai,[3,5] K. M. Kojima,[3] G. M. Luke,[2,3] and R. P. Singh[1,*]

[1]*Department of Physics, Indian Institute of Science Education and Research Bhopal, Bhopal 462066, India*
[2]*Department of Physics and Astronomy, McMaster University, Hamilton, Ontario, Canada L8S 4M1*
[3]*TRIUMF, Vancouver, British Columbia, Canada V6T 2A3*
[4]*Department of Physics, Sungkyunkwan University, Suwon 16419, Korea*
[5]*Quantum Matter Institute, The University of British Columbia, Vancouver, British Columbia, Canada V6T 1Z4*

(Received 15 February 2023; accepted 10 May 2023; published 19 May 2023)

Valence-skipped superconductors are natural candidates for unconventional superconductivity because they can exhibit a negative effective, attractive interaction for electron pairing. This work reports comprehensive x-ray diffraction, magnetization, specific heat, and muon spin rotation and relaxation measurements (μSR) on the valence-skipped compound $AgSnSe_2$. The temperature dependences of the electronic specific heat [$C_{el}(T)$] and the upper critical field [$H_{c2}(T)$] provide evidence of two-gap superconductivity, which is also confirmed by our transverse-field μSR measurements. Zero-field μSR measurements reveal at most a slight increase [$\sim 0.002(1)\ \mu s^{-1}$] in relaxation in the superconducting state, much less than reported in a range of superconductors with broken time-reversal symmetry. Further measurements with greatly improved statistics will be required to make a definitive determination of the possible presence of broken time-reversal symmetry.

DOI: 10.1103/PhysRevB.107.174517

I. INTRODUCTION

Understanding the microscopic pairing mechanism of unconventional superconductors is one of the most challenging problems in condensed matter physics. It has recently attracted much interest due to its possible applications in quantum technologies. In unconventional superconductors, the electron-pair formation is not mediated by phonons but by different mechanisms, including charge, spin, and magnetic fluctuations [1–3].

Valence-skipped materials are an exciting class of materials which may become unconventional superconductors. In these materials, due to valence skipping/valence fluctuations, negative-U centers are formed, which causes an attractive on-site interaction between the electrons [4–8] and promotes superconductivity with a relatively high T_c compared to conventional superconductors [9–14]. This valence-skipped induced negative-U superconductivity was previously proposed in Tl-doped PbTe and K- and Na-doped $BaBiO_3$ [15–17], with a high T_c value. Valence-skipped materials exhibit intriguing unconventional properties and other quantum phenomena, including charge density waves, pseudogaps, and the charge Kondo effect [3,4,18]. However, these valence-skipped compounds' exact superconducting pairing mechanism is still elusive. With the possibility of achieving a high value of T_c in relatively low carrier density materials, a valance-skipped superconducting pairing mechanism could be a novel route to realize high-T_c materials, motivating detailed microscopic studies which are not currently available for these materials.

The metal chalcogenide superconductor $AgSnSe_2$, where Ag partially substitutes Sn in SnSe, is a novel valence-skipped system [19,20]. The *ab initio* band structure calculations indicate SnSe is a nontrivial crystalline topological insulator [21,22]. X-ray absorption and x-ray photoemission spectroscopy studies of $AgSnSe_2$ suggested the presence of valency states Sn^{2+} and Sn^{4+}, which might create dynamic negative-U centers and contribute to superconductivity [23]. Further, ^{119}Sn Mössbauer spectroscopy suggests valence skip behavior with excess Sn [24]. The coexisting superconductivity and nontrivial band topology in $AgSnSe_2$ make it a unique valence-skipped system and motivate further studies of this compound. A thorough microscopic investigation requires understanding the correlation between unconventional superconductivity, valence fluctuations, and the effect of nontrivial band topology on the superconducting ground state of $AgSnSe_2$ and valence-skipped compounds in general.

In this paper, we report the bulk and microscopic superconducting properties of $AgSnSe_2$ via magnetization, specific heat, and muon spin rotation and relaxation (μSR) measurements. Our measurements confirm the superconducting transition temperature $T_c = 4.91(2)$ K. Transverse-field (TF) μSR measurements, along with the temperature dependence of the specific heat and the upper critical field, suggest a two isotropic ($s + s$) superconducting gap structure. Furthermore, zero-field (ZF) μSR measurements indicate that within our resolution, a small increase in Λ is observed in the superconducting state of $AgSnSe_2$.

II. EXPERIMENTAL DETAILS

The polycrystalline sample was synthesized using the solid-state reaction method. The required elemental powders of Ag (99.999%), Sn (99.99%), and Se (99.999%) were mixed in a stoichiometric ratio. The mixture was then palletized and heated at 800 °C for 48 h in a vacuum-sealed tube, followed

*rpsingh@iiserb.ac.in

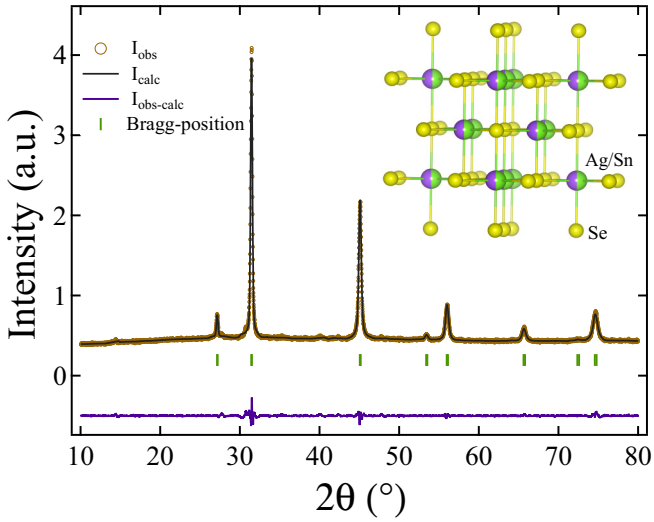

FIG. 1. Refined room temperature powder XRD pattern of $AgSnSe_2$; the inset shows the NaCl crystal structure with equal probability of occupying an edge state by Ag and Sn atoms.

by water quenching. At room temperature, the powder x-ray diffraction (XRD) pattern was collected using a PANalytical diffractometer equipped with Cu K_α radiation ($\lambda = 1.5406$ Å). Magnetic measurements were performed using a Quantum Design MPMS XL superconducting quantum interference device magnetometer with a reciprocating sample option (RSO) insert, and for measurements down to 0.5 K, an IQuantum He^3 insert was used. A physical property measurement system (Quantum Design) was used to measure the specific heat of the sample. Zero-field and transverse-field μSR measurements were performed at TRIUMF, Center for Molecular and Materials Science, Vancouver, Canada [25]. The applied magnetic field was perpendicular to the initial muon spin direction in the TF geometry. The μSR data were analyzed using the MUSRFIT software [26].

III. RESULTS AND DISCUSSION

The crystal structure of $AgSnSe_2$ is shown in the inset of Fig. 1, which depicts the partial substitution of Ag at the Sn site in SnSe. The Rietveld refined powder XRD pattern of $AgSnSe_2$ is shown in Fig. 1, confirming the crystallization in a cubic NaCl structure with the Fm-$3m$ space group. The obtained lattice parameters from the refinement, $a = b = c = 5.6865(2)$ Å, are in good agreement with previously reported values [27].

A. Magnetization

The temperature-dependent magnetic measurements are performed in zero-field-cooled warming (ZFCW) and field-cooled cooling (FCC) modes under 1 mT magnetic field, as shown in Fig. 2(a). The observed superconducting transition temperature of $AgSnSe_2$, $T_c = 4.91(2)$ K, is close to previously reported values [19,20]. The separation between ZFCW and FCC curves indicates the presence of strong flux pinning. The magnetization variation under a high magnetic field at a temperature of 1.8 K [inset of Fig. 2(a)] also suggests strong pinning with a complex vortex nature as a small area under the magnetization loop with the fishtail effect is observed [28]. An irreversible magnetic field is observed at $H_{irr} = 0.41(1)$ T, above which vortices start to unpin.

The field-dependent magnetization measurements at different temperatures below T_c estimate the lower critical field value. We performed the magnetization measurements on a spherical sample piece, allowing accurate demagnetizing field determination. We calculate the internal field of the sample by using $H_{internal} = H_{applied} - NM$, where $N = 1/3$ is the demagnetizing factor of a sphere and M is the magnetization [29]. The inset in Fig. 2(b) shows the variation of M versus $H_{internal}$, and the point of linear deviation in the low-field region is considered to be H_{c1} for the respective isotherm. The temperature dependence of the lower critical field H_{c1} is well described using the Ginzburg-Landau (GL) equation,

$$H_{c1}(T) = H_{c1}(0)\left[1 - \left(\frac{T}{T_c}\right)^2\right], \tag{1}$$

where the lower critical field is estimated to be $H_{c1}(0) = 5.76(6)$ mT [Fig. 2(b)].

From the magnetization measurement, the shift in T_c to a lower value with an increasing magnetic field is noted to ex-

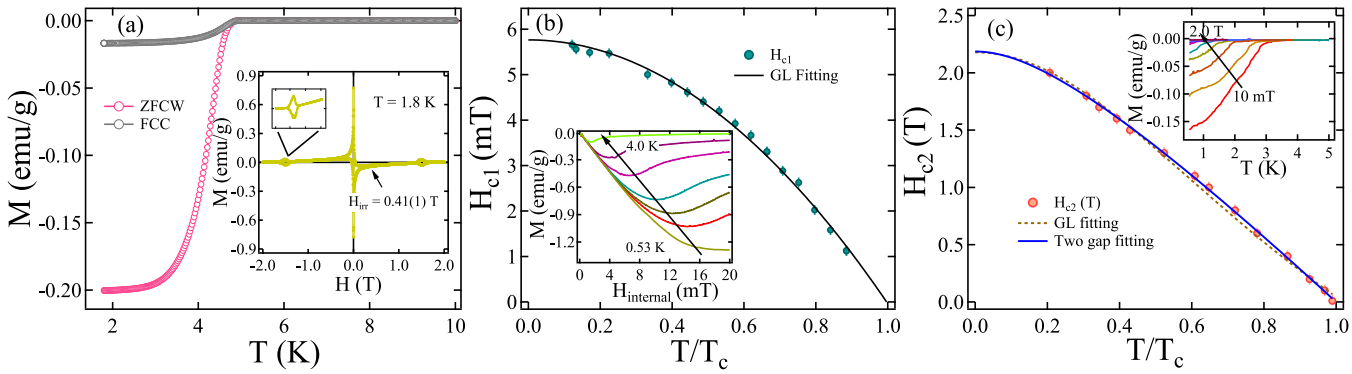

FIG. 2. (a) The magnetic measurements under ZFCW and FCC modes, with the magnetic hysteresis loop at 1.8 K in the inset. (b) The temperature variation of the lower critical field; the inset shows the M dependence on the internal magnetic field. (c) The upper critical field temperature variation fitted by the GL equation and the two-gap model are represented by dashed and solid lines, respectively. The inset shows the temperature-dependent magnetization at the different applied fields.

tract the upper critical field [inset in Fig. 2(c)]. We attempted to fit the H_{c2} versus T curve using the GL equation,

$$H_{c2}(T) = H_{c2}(0)\left[\frac{(1-t^2)}{(1+t^2)}\right], \tag{2}$$

where $t = T/T_c$ is the reduced temperature. Figure 2(c) shows the relatively poor fitting of the H_{c2} curve from the single-band GL model providing $H_{c2}^{\mathrm{GL}}(0) = 2.13(3)$ T. Therefore, a two-band model was used to analyze the H_{c2} variation. The two-band equation for the upper critical field is written in the parametric form as [30–34]

$$\ln t = -\frac{1}{2}\left[U(s) + U(\eta s) + \frac{\lambda_0}{w}\right] + \left(\frac{1}{4}\left[U(s) - U(\eta s) - \frac{\lambda_-}{w}\right]^2 + \frac{\lambda_{12}\lambda_{21}}{w^2}\right)^{1/2}, \tag{3}$$

where

$$U(s) = \psi\left(s + \frac{1}{2}\right) - \psi\left(\frac{1}{2}\right), \tag{4}$$

$H_{c2} = \frac{2\Phi_0 T s}{D_1}$, $\eta = \frac{D_2}{D_1}$, and the parameter s changes from 0 to 1 as T varies from T_c to 0. The variables $\lambda_{11}, \lambda_{22}, \lambda_{12}$, and λ_{21} are the matrix elements of the BCS coupling constants; $\lambda_- = \lambda_{11} - \lambda_{12}$, $\lambda_0 = (\lambda_-^2 + 4\lambda_{12}\lambda_{21})^{1/2}$, and $w = \lambda_{11}\lambda_{22} - \lambda_{21}\lambda_{12}$. D_1 and D_2 are the diffusivities of the two bands, while Φ_0 is the magnetic flux quantum and ψ is the digamma function. The fit of the H_{c2} curve using the two-band theory yields $H_{c2}^{2G}(0) = 2.18(7)$ T. The values of the upper critical field obtained from the two theories are much smaller than the Pauli paramagnetic limit, expressed as $H_{c2}^{P}(0) = 1.86T_c = 9.13(3)$ T [35,36]. Further, Ren *et al.* [20] reported the anomalous broadening of the magnetic-field-induced resistive transition and an increase in the upper critical field value in the low-temperature region in $AgSnSe_2$ which might be associated with the presence of multiple superconducting gaps, as suggested by our upper critical field results and also observed in MgB_2 [37].

We can evaluate various superconducting parameters using our H_{c2} and H_{c1} values. The superconducting coherence length $\xi_{\mathrm{GL}}(0)$ is calculated using GL theory as [29] $H_{c2}(0) = (\frac{\Phi_0}{2\pi\xi_{\mathrm{GL}}(0)^2})$, providing $\xi_{\mathrm{GL}}(0) = 12.2(4)$ nm. The London penetration depth λ_{GL} is obtained from the lower critical field $H_{c1}(0)$ using the expression [38]

$$H_{c1}(0) = \frac{\Phi_0}{4\pi\lambda_{\mathrm{GL}}^2(0)}\left(\ln\frac{\lambda_{\mathrm{GL}}(0)}{\xi_{\mathrm{GL}}(0)} + 0.12\right), \tag{5}$$

which gives $\lambda_{\mathrm{GL}}(0) = 309(13)$ nm for $H_{c1}(0) = 2.07(1)$ mT and $\xi_{\mathrm{GL}}(0) = 12.2(4)$ nm. The GL parameter, $\kappa_{\mathrm{GL}} = \lambda_{\mathrm{GL}}(0)/\xi_{\mathrm{GL}}(0) = 25(2)$, indicates the strong type-II superconducting nature of $AgSnSe_2$. Using these parameters and the relation $H_{c1}H_{c2} = H_c^2 \ln\kappa_{\mathrm{GL}}$ [38], the thermodynamic critical field value $H_c(0) = 62(7)$ mT is also estimated.

B. Specific heat

The temperature-dependent specific heat of $AgSnSe_2$ under zero magnetic field is shown in Fig. 3(a). The significant

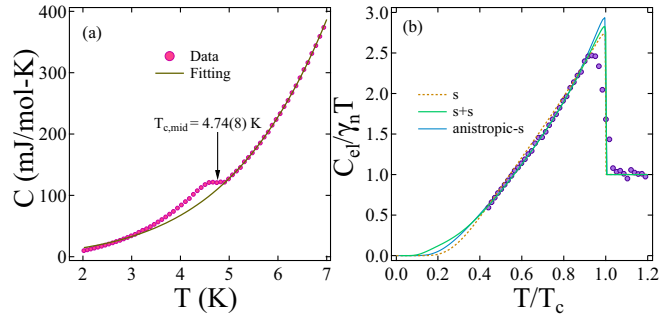

FIG. 3. (a) Specific heat fitting in the normal region. (b) Fitted data for normalized electronic specific heat $C_{\mathrm{el}}/\gamma_n T$ using the isotropic and anisotropic s-wave models, indicated by the dotted yellow and solid blue lines, respectively, and the two-gap $(s+s)$-wave model, indicated by the solid green line.

jump in the specific heat around temperature $T_{c,\mathrm{mid}} = 4.74(8)$ K further confirms the bulk nature of superconductivity in the sample. The normal-state specific heat above T_c was fit by the Debye relation,

$$C = \gamma_n T + \beta_3 T^3 + \beta_5 T^5, \tag{6}$$

where $\gamma_n T$ is the electronic contribution, $\beta_3 T^3$ is the phononic contribution, and $\beta_5 T^5$ is the anharmonic contribution in the specific heat. The best fit to the data yields Sommerfeld coefficient $\gamma_n = 4.6(1)$ mJ mol^{-1} K^{-2}, Debye constant $\beta_3 = 0.68(1)$ mJ mol^{-1} K^{-4}, and $\beta_5 = 7.5(1)$ μJ mol^{-1} K^{-5}.

Further, γ_n is used to evaluate the density of states at the Fermi level $D_C(E_{\mathrm{F}})$ via the relation $\gamma_n = (\frac{\pi^2 k_B^2}{3})D_C(E_{\mathrm{F}})$, where $k_B = 1.38 \times 10^{-23}$ J K^{-1}. $D_C(E_{\mathrm{F}})$ is calculated to be 1.97(6) states eV^{-1} f.u.$^{-1}$. The Debye temperature is obtained from β_3 using the expression $\theta_D = (\frac{12\pi^4 RN}{5\beta_3})^{\frac{1}{3}} = 255(3)$ K, where $R = 8.314$ J mol^{-1} K^{-1} is the gas constant. The electron-phonon coupling constant $\lambda_{e\text{-ph}}$ can be calculated from the inverted McMillan's equation [39],

$$\lambda_{e\text{-ph}} = \frac{1.04 + \mu^* \ln(\theta_D/1.45T_c)}{(1 - 0.62\mu^*)\ln(\theta_D/1.45T_c) - 1.04}, \tag{7}$$

where μ^* is the screened Coulomb repulsion and is taken to be 0.13. For $\theta_D = 255$ K and $T_{c,\mathrm{mid}} = 4.74$ K, $\lambda_{e\text{-ph}} = 0.69(1)$. The obtained value of $\lambda_{e\text{-ph}}$ is in the range of moderately coupled superconductors.

To evaluate the superconducting gap parameter, we analyzed the electronic specific heat below T_c. The electronic contribution is extracted by subtracting the lattice contribution from the total specific heat. The normalized superconducting gap $\Delta(0)/k_B T_c$ is estimated by fitting the data to the BCS expectation of electronic specific heat, which is expressed as [40]

$$\frac{C_{\mathrm{el}}}{\gamma_n T_c} = t\frac{d}{dt}\left[\frac{-6\Delta(0)}{\pi^2 k_B T_c}\int_0^\infty [f\ln(f) + (1-f)\ln(1-f)]dy\right], \tag{8}$$

where $t = T/T_c$, $f(\xi) = \{\exp[E(\xi)/k_B T] + 1\}^{-1}$ is the Fermi function, and $E(\xi) = \sqrt{\xi^2 + \Delta^2(t)}$, with $E(\xi)$ being the energy of the normal electrons measured relative to the Fermi energy. $y = \xi/\Delta(0)$ and $\Delta(t) = \tanh(1.82\{1.018[(1/t) -$

1]})$^{0.51}$ is the BCS approximation for the temperature dependence of the energy gap. The normalized $C_{\rm el}(T)$ fitting deviates from a single s-wave model, as shown in the Fig. 3(b), whereas an anisotropic s-wave model and a two-gap isotropic $s+s$ model fit the data better. The anisotropic s-wave model described in Ref. [41] is used along with the two-gap model used in other multigap superconductors such as MgB_2 [42], $Lu_2Fe_3Si_5$ [43], and La_7Ni_3 [44]. In the two-gap model, the two parameters $\Delta_1(0)/k_BT_c$ and $\Delta_2(0)/k_BT_c$ correspond to the two different superconducting gaps, and the weighted contribution x of the partial Sommerfeld coefficient is the third fitting parameter involved. The best fit of the data from the two-gap $s+s$ model yields $x = 0.17(6)$, $\Delta_1(0)/k_BT_c = 0.80(8)$, and $\Delta_2(0)/k_BT_c = 2.16(3)$, whereas the anisotropic s-wave model gives $\Delta(0)/k_BT_c = 2.70(5)$ and $a = 0.37(4)$ [Fig. 3(b)]. In the two-gap model, a significant difference in the two gap values and the gap ratio $\frac{\Delta_2(0)}{\Delta_1(0)} \simeq 2.7(3)$ is observed with the smaller gap, with Δ_1 making a relatively weak contribution (0.17) to the superconducting state. The larger gap value, $\Delta_2(0)/k_BT_c = 2.16$, is higher than the BCS value in the weak coupling limit, suggesting strong electron-phonon coupling in $AgSnSe_2$. A previous report on polycrystalline $AgSnSe_2$ reported a single isotropic gap (also somewhat larger than that expected in the weak coupling limit of BCS theory); it is possible that the apparent absence of a two-gap nature in that study might be due to sample differences or could indicate that a multigap analysis was not performed [20]. Furthermore, the two-gap $s+s$ model and the anisotropic s model both fit the data well [Fig. 3(b)]. They are indistinguishable, as there is only a slight difference in the estimated gap values. However, low-temperature specific heat data are required to distinguish between the two models.

C. Muon spin rotation and relaxation

To further understand the superconducting gap structure of the valence-skipped superconductor $AgSnSe_2$ at the microscopic level, we carried out transverse-field μSR measurements. The measurements were performed using the field-cooled protocol in a field of 0.1 T. Representative TF asymmetry spectra above and below T_c are plotted in a rotating reference frame of 0.095 T for clarity, as shown in Fig. 4(a), where a clear difference between the two is observable. Below T_c, the precession signal shows significant damping with time due to the inhomogeneous field distribution from the flux-line lattice in the mixed state. The time domain spectra were fit to analyze the temperature dependence of superconducting parameters. The TF asymmetry spectra are described by two sinusoidally oscillating functions, with the Gaussian decaying component characterizing the sample signal and a temperature-independent weakly decaying exponential component characterizing the background signal,

$$A_{\rm TF}(T) = A\left[F\exp\left(\frac{-\sigma^2t^2}{2}\right)\cos(wt+\phi) + (1-F)\exp(-\sigma_{bg})\cos(w_{bg}t+\phi)\right], \quad (9)$$

where ϕ is the initial phase of the muons entering the sample and A is the total TF asymmetry. F is the fraction of the signal

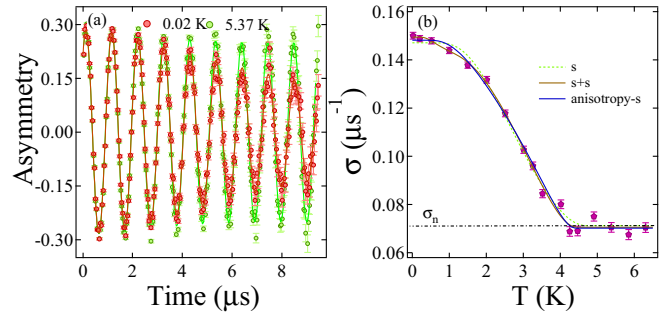

FIG. 4. (a) Transverse-field spectra recorded in an applied magnetic field of 0.1 T at temperatures 5.37 K ($>T_c$) and 0.02 K ($<T_c$) plotted in a rotating reference frame of 0.095 T, where solid lines are the fits using Eq. (9). (b) Temperature dependence of the total relaxation rate σ. The dashed line represents the s-wave fitting; the solid blue and brown lines represent the anisotropic s and two isotropic $(s+s)$-wave models, respectively, and σ_n is the nuclear relaxation rate in the normal state (above T_c).

coming from the sample, and w and w_{bg} are the frequencies of the oscillatory muon signal in the sample and background, respectively. σ is the total Gaussian muon relaxation rate. Above the transition temperature T_c, σ becomes temperature independent, reflecting the nuclear contribution in the normal state called σ_n [represented by a horizontal dot-dashed line in Fig. 4(b)]. The total relaxation rate σ consists of contributions from both the superconducting and nuclear parts and can be written as

$$\sigma^2 = \sigma_{\rm sc}^2 + \sigma_n^2, \quad (10)$$

where $\sigma_{\rm sc}$ is the relaxation in the vortex state.

The temperature dependence of the superconducting muon depolarization rate $\sigma_{\rm sc}$ can be expressed in the semiclassical approximation as

$$\frac{\sigma_{\rm sc}(T,\Delta_{0,i})}{\sigma_{\rm sc}(0,\Delta_{0,i})} = \frac{\lambda_{\rm sc}^{-2}(T,\Delta_{0,i})}{\lambda_{\rm sc}^{-2}(0,\Delta_{0,i})} = 1+\frac{1}{\pi}\int_0^{2\pi}\int_{\Delta(T,\phi)}^{\infty}\left(\frac{\delta f}{\delta E}\right)\frac{EdEd\phi}{\sqrt{E^2-\Delta_i(T,\phi)^2}}, \quad (11)$$

where $f(E) = [1+\exp(E/k_BT)]^{-1}$ is the Fermi function and $\Delta_i(T,\phi) = \Delta_{0,i}\delta(T/T_c)g(\phi)$. The temperature variation $\delta(T/T_c) = \tanh\{1.82[1.018(T_c/T-1)]^{0.51}\}$, and $g(\phi)$ refers to the angular dependence of the superconducting gap function with azimuthal angle ϕ. For an isotropic s-wave gap, $g(\phi)$ becomes equal to 1, whereas for an anisotropic s-wave gap, $g(\phi) = [1+a\cos(4\phi)]/(1+a)$, where a is the anisotropic parameter [41]. Combining Eqs. (10) and (11), the σ variation with temperature can be fitted with σ_n as a fitting parameter. The σ versus T curve fitted with various models is shown in Fig. 4(b). Both isotropic and anisotropic s-wave models with gap values $\Delta_0 = 0.68(5)$ and 1.12(4) meV [and $a = 0.66(6)$] and $\chi^2 = 1.43$ and 1.37, respectively, do not properly fit the temperature variation of σ. Hence, a function consisting of a weighted linear combination of two distinct superconducting gaps is considered and corresponds to the model used to fit the

specific heat data [43,44],

$$\frac{\sigma_{sc}(T)}{\sigma_{sc}(0)} = x\frac{\sigma_{sc}(T,\Delta_{0,1})}{\sigma_{sc}(0,\Delta_{0,1})} + (1-x)\frac{\sigma_{sc}(T,\Delta_{0,2})}{\sigma_{sc}(0,\Delta_{0,2})}, \quad (12)$$

where $\Delta_{0,1}$ and $\Delta_{0,2}$ are the two gap values, respectively, and x is the weighting factor, measuring the relative contributions to superconducting parameters. The two-gap ($s+s$)-wave model fits better than the single gap s-wave model for $x = 0.20(4)$, with respective gap values of $\Delta_{0,1}(0) = 0.29(6)$ meV $[\Delta_{0,1}(0)/k_BT_c = 0.77(9)]$ and $\Delta_{0,2}(0) = 0.80(5)$ meV $[\Delta_{0,2}(0)/k_BT_c = 2.12(5)]$ and $\chi^2 = 1.25$ [Fig. 4(b)]. The ratio of superconducting gaps $\frac{\Delta_{0,2}(0)}{\Delta_{0,1}(0)} \simeq 2.7(5)$ is consistent with the value estimated from the specific heat measurement. Furthermore, in the low-temperature region, a noticeable difference is observed between the anisotropic s and two-gap $s+s$ fits, which is not apparent in the specific heat data. This confirms the two-gap nature of our sample.

For an ideal vortex lattice, the relation between the magnetic penetration depth λ and the superconducting depolarization rate σ_{sc} for the GL parameter $\kappa \geqslant 5$ is given by [45,46]

$$\frac{\sigma_{sc}^2(T)}{\gamma_\mu^2} = \frac{0.00371\Phi_0^2}{\lambda^4(T)}, \quad (13)$$

where $\gamma_\mu/2\pi = 135.5$ MHz/T is the muon gyromagnetic ratio and $\Phi_0 = 2.068 \times 10^{-15}$ Wb is the magnetic flux quantum. The estimated magnetic penetration depth at $T = 0$ K is $\lambda(0) = 901(35)$ nm. The obtained value is significantly different from the value estimated from magnetization; such a large difference in λ has also been observed in some other compounds [47,48] and is not well understood. It is possible that the disagreement could represent a true difference in determining the penetration depth from the lower critical field (in the Meissner state) and from the superfluid density (in the vortex state).

To further investigate the superconducting ground state of $AgSnSe_2$, ZF-μSR measurements were performed. The ZF-μSR time domain spectra were measured at various temperatures on either side of the superconducting transition temperature. Figure 5 shows representative asymmetry spectra above and below T_c. The ZF-μSR spectra were analyzed by fitting the time-domain asymmetry variation using the damped Gaussian Kubo-Toyabe function G_{KT} [49],

$$A(t) = A_0[fG_{KT}(t) + (1-f)]\exp(-\Lambda t) + A_{BG}, \quad (14)$$

where

$$G_{KT}(t) = \frac{1}{3} + \frac{2}{3}(1-\Delta^2t^2)\exp\left(\frac{-\Delta^2t^2}{2}\right) \quad (15)$$

and A_0 and A_{BG} are the initial asymmetries corresponding to the sample and the background, respectively. The above expression takes into account the relaxation effect on muons due to two distinct environments: (1) muons located at sites near atoms with nuclear moments, which follow a Gaussian Kubo-Toyabe function with a fraction of f, and (2) muons near atoms without nuclear moments, which exhibit a nonrelaxing term (second term in parentheses). This fit is mandated since most atoms have zero or very small nuclear magnetic moments (7.6% of Se atoms have a nonzero nuclear magnetic moment $0.53\mu_N$, 16.3% of Sn atoms have a nonzero moment of approximately $1.0\mu_N$, and Ag has an almost zero nuclear moment of $0.1\mu_N$). These terms are then multiplied by a temperature-dependent exponential decay ($\exp -\Lambda t$), which characterizes any relaxation due to potential time-reversal symmetry-breaking magnetic fields. The Kubo-Toyabe Δ characterizes the temperature-independent muon spin relaxation due to the randomly oriented, static nuclear moments. The inset in Fig. 5 shows the temperature dependence of Λ. A slight increase below T_c would indicate the presence of time-reversal symmetry breaking. We can estimate the largest such time-reversal-symmetry field that could be present by fitting $\Lambda(T)$ to the order-parameter form $\Lambda(T) = \Lambda(T = 0) * [1 - (T/T_c)^2]$. Such a fit gives a maximum time-reversal-symmetry field relaxation rate $\Lambda(0) = 0.002(1)\,\mu s^{-1}$, where the 50% uncertainty in the relaxation rate represents the statistic uncertainty. This relaxation rate is significantly lower than those reported for any time-reversal symmetry-breaking superconductors reported to date [50–52] and is statistically almost consistent with zero; unknown systematic errors could further increase this uncertainty, giving a possible relaxation rate consistent with zero. Further investigations with much higher statistics at additional temperatures will be necessary to definitively clarify the presence of broken time-reversal symmetry in the superconducting ground state.

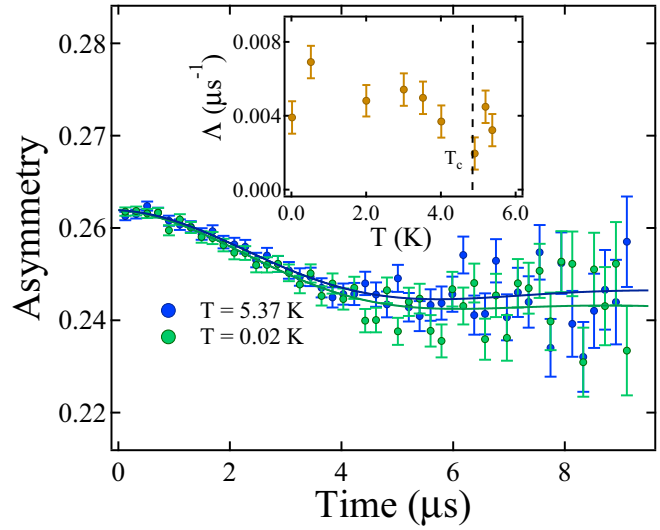

FIG. 5. Zero-field asymmetry spectra collected below ($T = 0.02$ K) and above ($T = 5.37$ K) the transition temperature T_c, where the solid lines represent the fit to the data using Eqs. (14) and (15). The inset shows the temperature variation of the electronic relaxation rate Λ.

We can use Uemura's classification scheme [53] to place $AgSnSe_2$ in the context of other superconductors based on the ratio of T_c/T_F. For unconventional superconductors, the ratio generally falls to $0.01 \leqslant T_c/T_F \leqslant 0.1$; however, for conventional superconductors, $T_c/T_F \leqslant 0.0003$. The effective Fermi temperature T_F of $AgSnSe_2$ is extracted by considering the 3D Fermi surface expression [54]

$$k_BT_F = \frac{\hbar^2}{2}(3\pi^2)^{2/3}\frac{n^{2/3}}{m^*}, \quad (16)$$

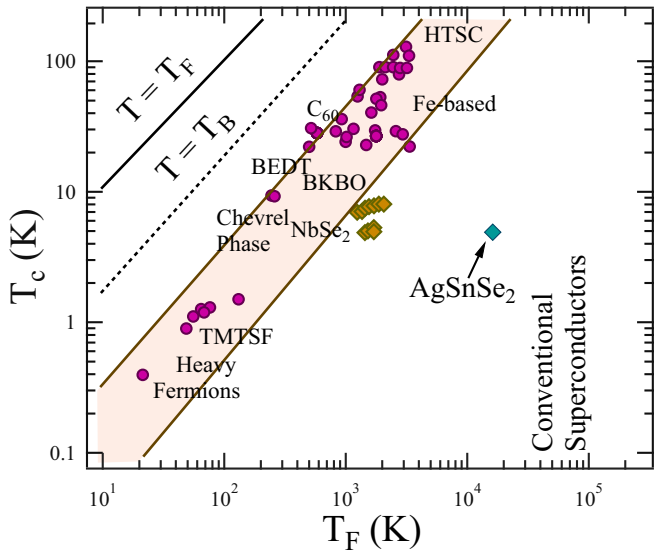

FIG. 6. A plot between the superconducting transition temperature T_c and the effective Fermi temperature T_F for $AgSnSe_2$. The data points in the shaded region represent the band of unconventionality [60,61].

where n is the carrier density and m^* is the effective mass. m^* is calculated from the Sommerfeld coefficient via the relation $m^* = (\hbar k_F)^2 \gamma_n / \pi^2 n k_B^2$, where $\gamma_n = 84.51$ J m^{-3} K^{-2}, k_F is the Fermi vector, and n is taken from Ref. [20]. The estimated value $T_F = 16200(610)$ K places $AgSnSe_2$ well outside the unconventional superconductor band, close to conventional superconductors, as shown in Fig. 6.

Doping with valency-skipped elements can enhance or induce superconductivity in low carrier density systems such as topological semimetals and semiconductors. This could be a prototype for realizing a new quantum phase called topological superconductivity (TSC), in which the topological phase and superconductivity coexist [55]. An example is In-doped SnTe, a possible topological superconductor, in which the valence-skipped state of In induces superconductivity in the topological crystalline insulator SnTe [56,57]. Moreover, Ag-doped SnSe and other systems, including In-doped GeTe and K-doped $BaBiO_3$, exhibit nontrivial topological band structures [58,59]. Thus, the aforementioned material corresponds to the category of possible topological superconductors and presents $AgSnSe_2$ as a candidate for TSC. However, detailed studies and band structure calculations are required to investigate the origin of multigap superconductivity and to address the effect of the nontrivial band topology with the possible negative-U induced superconductivity in $AgSnSe_2$.

IV. CONCLUSION

In conclusion, our study has confirmed the bulk superconductivity of $AgSnSe_2$ with a transition temperature of 4.91(2) K through detailed magnetization and specific heat measurements (Table I). Our microscopic investigations using muon spin rotation and relaxation measurements have revealed the presence of two isotropic $s+s$ superconducting gaps, a finding supported by the temperature variation of specific heat and upper critical field measurements. Zero-field μSR measurements revealed at most a slight increase [$\sim$0.002(1) μs^{-1}] in relaxation in the superconducting state, much less than reported in a range of superconductors with broken time-reversal symmetry. Further measurements with greatly improved statistics will be required to make a definitive determination of the possible presence of broken time-reversal symmetry. In addition, more investigation is necessary to determine whether the attractive interaction between electrons is mediated via negative U due to valence skipping/valence fluctuations or some other non-BCS pairing mechanism. Furthermore, the role of nontrivial topological states in the superconducting ground state of the valence-skipped compound requires further exploration.

TABLE I. Parameters in the superconducting and normal states of $AgSnSe_2$.

Parameter	Units	$AgSnSe_2$
T_C	K	4.91(2)
$H_{c1}(0)$	mT	5.76(6)
$H_{c2}^{GL}(0)$	T	2.13(3)
$H_{c2}^{2G}(0)$	T	2.18(7)
$H_{c2}^{P}(0)$	T	9.13(3)
$\xi_{GL}(0)$	nm	12.2(4)
$\lambda_{GL}(0)$ (Magnetization)	nm	309(13)
$\lambda(0)$ (μSR)	nm	907(35)
$\kappa_{GL}(0)$		25(2)
γ_n	mJ mol^{-1} K^{-2}	4.6(1)
θ_D	K	255(3)
$\lambda_{e\text{-ph}}$		0.69(1)
Δ_2/Δ_1^{SH}		2.7(3)
$\Delta_2/\Delta_1^{\mu SR}$		2.7(5)
T_F	K	16200(610)
T_c/T_F		0.0003(1)
m^*/m_e		1.88(2)

ACKNOWLEDGMENTS

A.K. acknowledges the funding agency Council of Scientific and Industrial Research (CSIR), Government of India, for providing a SRF fellowship [Award No. 09/1020(0172)/2019-EMR-I]. R.P.S. acknowledges the Science and Engineering Research Board, Government of India, for the CRG/2019/001028 Core Research Grant. G.M.L. (McMaster) acknowledges the support of the Natural Sciences and Engineering Research Council (Canada).

[1] T. Moriya and K. Ueda, Rep. Prog. Phys. **66**, 1299 (2003).

[2] G. Aeppli, E. Bucher, C. Broholm, J. K. Kjems, J. Baumann, and J. Hufnagl, Phys. Rev. Lett. **60**, 615 (1988).

[3] P. B. Littlewood, Phys. B (Amsterdam, Neth.) **163**, 299 (1990).
[4] A. Taraphder and P. Coleman, Phys. Rev. Lett. **66**, 2814 (1991).
[5] A. Taraphder, H. R. Krishnamurthy, R. Pandit, and T. V. Ramakrishnan, Phys. Rev. B **52**, 1368 (1995).
[6] I. O. Kulik and A. G. Pedan, Phys, B+C (Amsterdam, Neth.) **107**, 665 (1981).
[7] C. M. Varma, Phys. Rev. Lett. **61**, 2713 (1988).
[8] P. W. Anderson, Phys. Rev. Lett. **34**, 953 (1975).
[9] K. D. Tsendin and B. P. Popov, Supercond. Sci. Technol. **12**, 255 (1999).
[10] R. Micnas, J. Ranninger, and S. Robaszkiewicz, Rev. Mod. Phys. **62**, 113 (1990).
[11] J. E. Hirsch and D. J. Scalapino, Phys. Rev. B **32**, 5639 (1985).
[12] H. U. R. Strand, Phys. Rev. B **90**, 155108 (2014).
[13] T. Yanagisawa and I. Hase, Phys. C (Amsterdam, Neth.) **494**, 24 (2013).
[14] A. N. Kocharian and C. Yang, Mater. Chem. Phys. **42**, 134 (1995).
[15] S. A. Nemov and Y. I. Ravich, Phys. Usp. **41**, 735 (1998).
[16] I. Hase and T. Yanagisawa, Phys. Rev. B **76**, 174103 (2007).
[17] R. J. Cava, B. Batlogg, J. J. Krajewski, R. Farrow, L. J. Rupp, A. E. White, and T. Kometani, Nature (London) **332**, 814 (1988).
[18] M. Dzero and J. Schmalian, Phys. Rev. Lett. **94**, 157003 (2005).
[19] D. C. Johnston and H. Adrian, J. Phys. Chem. Solids **38**, 355 (1977).
[20] Z. Ren, M. Kriener, A. A. Taskin, S. Sasaki, K. Segawa, and Y. Ando, Phys. Rev. B **87**, 064512 (2013).
[21] Y. Sun, Z. Zhong, T. Shirakawa, C. Franchini, D. Li, Y. Li, S. Yunoki, and X. Q. Chen, Phys. Rev. B **88**, 235122 (2013).
[22] I. Tateishi and H. Matsuura, J. Phys. Soc. Jpn. **87**, 073702 (2018).
[23] T. Wakita, E. Paris, K. Kobayashi, K. Terashima, M. Y. Hacisalihoğlu, T. Ueno, F. Bondino, E. Magnano, I. Píš, L. Olivi L., and J. Akimitsu, Phys. Chem. Chem. Phys. **19**, 26672 (2017).
[24] F. S. Nasredinov, S. A. Nemov, V. F. Masterov, and P. P. Seregin, Phys. Solid State **41**, 1741 (1999).
[25] *Muon Science: Muons in Physics, Chemistry and Materials*, edited by S. L. Lee, S. H. Kilcoyne, and R. Cywinski (Taylor and Francis, Abingdon, UK, 1999), doi: 10.1201/9780203746196.
[26] A. Suter and B. M. Wojek, Phys. Procedia **30**, 69 (2012).
[27] A. Wold and R. Brec, Mater. Res. Bull. **11**, 761 (1976).
[28] D. A. Mayoh, J. A. T. Barker, R. P. Singh, G. Balakrishnan, D. M. Paul, and M. R. Lees, Phys. Rev. B **96**, 064521 (2017).
[29] M. Tinkham, *Introduction to Superconductivity*, 2nd ed. (McGraw-Hill, New York, 1996).
[30] C. Buzea and T. Yamashita, Supercond. Sci. Technol. **14**, R115 (2001).
[31] A. Gurevich, Phys. C (Amsterdam, Neth.) **456**, 160 (2007).
[32] J. Wang, X. Xu, N. Zhou, L. Li, X. Cao, J. Yang, Y. Li, C. Cao, J. Dai, J. Zhang, and Z. Shi, J. Supercond. Novel Magn. **28**, 3173 (2015).
[33] K. P. Sajilesh and R. P. Singh, Supercond. Sci. Technol. **34**, 055003 (2021).
[34] H. Suderow, V. G. Tissen, J. P. Brison, J. L. Martinez, and S. Vieira, Phys. Rev. Lett. **95**, 117006 (2005).
[35] B. S. Chandrasekhar, Appl. Phys. Lett. **1**, 7 (1962).
[36] A. M. Clogston, Phys. Rev. Lett. **9**, 266 (1962).
[37] P. Szabo, P. Samuely, A. G. M. Jansen, T. Klein, J. Marcus, D. Fruchart, and S. Miraglia, Phys. C (Amsterdam, Neth.) **369**, 250 (2002).
[38] T. Klimczuk, F. Ronning, V. Sidorov, R. J. Cava, and J. D. Thompson, Phys. Rev. Lett. **99**, 257004 (2007).
[39] W. L. McMillan, Phys. Rev. **167**, 331 (1968).
[40] H. Padamsee, J. E. Neighbor, and C. A. Shiffman, J. Low Temp. Phys. **12**, 387 (1973).
[41] R. Khasanov, K. Conder, E. Pomjakushina, A. Amato, C. Baines, Z. Bukowski, J. Karpinski, S. Katrych, H. H. Klauss, H. Luetkens, A. Shengelaya, and N. D. Zhigadlo, Phys. Rev. B **78**, 220510(R) (2008).
[42] F. Bouquet, Y. Wang, R. A. Fisher, D. G. Hinks, J. D. Jorgensen, A. Junod, and N. E. Phillips, Europhys. Lett. **56**, 856 (2001).
[43] P. K. Biswas, G. Balakrishnan, D. M. Paul, M. R. Lees, and A. D. Hillier, Phys. Rev. B **83**, 054517 (2011).
[44] Arushi, D. Singh, A. D. Hillier, M. S. Scheurer, and R. P. Singh, Phys. Rev. B **103**, 174502 (2021).
[45] E. H. Brandt, Phys. Rev. B **37**, 2349 (1988).
[46] E. H. Brandt, Phys. Rev. B **68**, 054506 (2003).
[47] V. K. Anand, D. T. Adroja, M. R. Lees, P. K. Biswas, A. D. Hillier, and B. Lake, Phys. Rev. B **98**, 214517 (2018).
[48] M. Mandal, C. Patra, A. Kataria, D. Singh, P. K. Biswas, J. S. Lord, A. D. Hillier, and R. P. Singh, Phys. Rev. B **104**, 054509 (2021).
[49] R. S. Hayano, Y. J. Uemura, J. Imazato, N. Nishida, T. Yamazaki, and R. Kubo, Phys. Rev. B **20**, 850 (1979).
[50] S. K. Ghosh, S. Kumar, M. Smidman, T. Shang, J. F. Annett, A. D. Hillier, J. Quintanilla, and H. Yuan, J. Phys.: Condens. Matter **33**, 033001 (2021).
[51] D. Singh, M. S. Scheurer, A. D. Hillier, D. T. Adroja, and R. P. Singh, Phys. Rev. B **102**, 134511 (2020).
[52] T. Shang, S. K. Ghosh, J. Z. Zhao, L.-J. Chang, C. Baines, M. K. Lee, D. J. Gawryluk, M. Shi, M. Medarde, J. Quintanilla, and T. Shiroka, Phys. Rev. B **102**, 020503(R) (2020).
[53] Y. J. Uemura *et al.* Phys. Rev. Lett. **62**, 2317 (1989).
[54] A. D. Hillier and R. Cywinski, Appl. Magn. Reson. **13**, 95 (1997).
[55] X. L. Qi and S. C. Zhang, Rev. Mod. Phys. **83**, 1057 (2011).
[56] M. Novak, Mario, S. Sasaki, M. Kriener, K. Segawa, and Y. Ando, Phys. Rev. B **88**, 140502(R) (2013).
[57] N. Haldolaarachchige, Q. Gibson, W. Xie, M. B. Nielsen, S. Kushwaha, and R. J. Cava, Phys. Rev. B **93**, 024520 (2016).
[58] M. Kriener, M. Sakano, M. Kamitani, M. S. Bahramy, R. Yukawa, K. Horiba, H. Kumigashira, K. Ishizaka, Y. Tokura, and Y. Taguchi, Phys. Rev. Lett. **124**, 047002 (2020).
[59] G. Li, B. Yan, R. Thomale, and W. Hanke, Sci. Rep. **5**, 10435 (2015).
[60] K. Hashimoto, K. Cho, T. Shibauchi, S. Kasahara, Y. Mizukami, R. Katsumata, Y. Tsuruhara, T. Terashima, H. Ikeda, M. A. Tanatar, H. Kitano, N. Salovich, R. W. Giannetta, P. Walmsley, A. Carrington, R. Prozorov, and Y. Matsuda, Science **336**, 1554 (2012).
[61] R. Khasanov, H. Luetkens, A. Amato, H. H. Klauss, Z. A. Ren, J. Yang, W. Lu, and Z. X. Zhao, Phys. Rev. B **78**, 092506 (2008).